CONFERENCE PRE-PRINT

OVERVIEW OF WEST CONTRIBUTIONS TO THE NEW ITER BASELINE AND FUSION POWER PLANTS

J. BUCALOSSI¹ AND THE WEST TEAM* CEA, IRFM, F-13108 Saint-Paul-lez-Durance, France *http://west.cea.fr/WESTteam email: jerome.bucalossi@cea.fr

Abstract

In 2023-2025, WEST has developed robust long pulse discharges and reached duration exceeding 1000s (record 1337s), using a predict first approach. Reliable machine operation was key to achieve those performances. WEST is equipped with a full actively cooled ITER grade divertor and has provided ITER relevant heat fluxes (up to 12 MW/m2) and particle fluence (over 1027 D/m2). Cracks have been observed on the top surface of the mono-blocks, but do not hamper the divertor power exhaust capability so far. Significant erosion has been observed in the strike point area while thick deposited layers build up on the high field side of the divertor. Those deposited layers are prone to flaking, leading to impurity ingress in the plasma. A laser cleaning procedure has been developed to remove those deposited layers. With the objective to mitigate tungsten erosion, a detached X-point radiator regime has been developed and controlled up to 34s duration. The transition into XPR was successfully modelled with the SOLEDGE code. WEST has also addressed urgent R&D issues in support to the tungsten first wall foreseen in the new ITER baseline, to inform the design of the ITER boronization system and characterize runaway impact. It was confirmed that glow discharge boronization (GDBs) is required to ensure a reliable plasma start-up. It was also shown that a non-uniform GDB is sufficiently efficient, and is less asymmetric than anticipated from modelling. WEST has also produced run-away beams up to 1.2s and studied their mitigation with new diagnostics. A dedicated run-away crash on the inboard limiter has been successfully achieved to validate the models of run-away damage in ITER. In the next two years, 3MW of ECRH will be made available on WEST to extend the operational domain to H-mode and control tungsten transport. Beyond 2027, WEST plans to increase pulse length at higher power by upgrading its first wall to an ITER like configuration.

1. INTRODUCTION

In the context of the new ITER baseline, the WEST programme has recently enhanced its efforts in supporting the goal of a robust start of the ITER scientific exploitation. The WEST super-conducting tokamak is a full tungsten wall long pulse device equipped with an actively cooled ITER grade divertor [1]. As such, it is best placed to address scientific and operational issues relevant to next step devices with a full tungsten (W) environment. For this purpose, WEST has developed reliable, routine and controlled long pulse regimes with durations now reaching 1337s with 2.6GJ of injected energy and exposed its actively cooled tungsten (W) divertor mono-blocks (MB) to heat flux up to 12MW/m2, beyond the nominal ITER heat load specifications (10MW/m2). Dedicated divertor melting experiments were also performed [2]. Since 2023, WEST has produced 3 campaigns, reaching a total of 18h cumulated plasma time on the divertor plates. Boron nitride limiters were replaced by tungsten components in 2025 to put WEST into a wall configuration mimicking the future ITER set-up. A high fluence campaign was also carried out with repetitive 60s pulses to study systematically the impact of heat and particle fluence on the divertor actively cooled components.

This paper reports on the key achievements of the past two years, namely: i) the making of long pulse discharges in WEST ii) the impact of high heat and particle flux on ITER grade plasma facing units (PFUs) iii) the plasma start-up in a full tungsten environment and the conditioning by GDCs mimicking the ITER set-up, iv) the progress in the X-point Radiator (XPR) controlled detached regime, and v) the contribution of WEST to ITER key issues such as run-away mitigations and isotope retention. This paper will also present the future developments of the machine capabilities.

2. THE MAKING OF LONG PULSES

From 2022 to 2024, discharge performance has continuously improved in terms of pulse length. The WEST tokamak confirmed its capability to operate routinely long pulse discharges: the number of discharges lasting more than 100s were increased by a factor of three between the four months plasma campaigns in 2023 (C6 & C7) and 2024 (C8 & C9) (figure 1), thanks to the non-inductive current drive capability from the Lower Hybrid Current Drive (LHCD) system. This was continued over the two months of the C10 campaign at the end of 2024 which produced a new record plasma duration of 824s with 1.93GJ (injected energy) (figure 2). In 2025, this effort culminated with a record pulse of 1337s and 2.62GJ of injected energy (figure 3).

2.1 Key technical system for achieving long pulse operation

The WEST performance is also demonstrated by the cumulated plasma duration reached over the last two campaigns

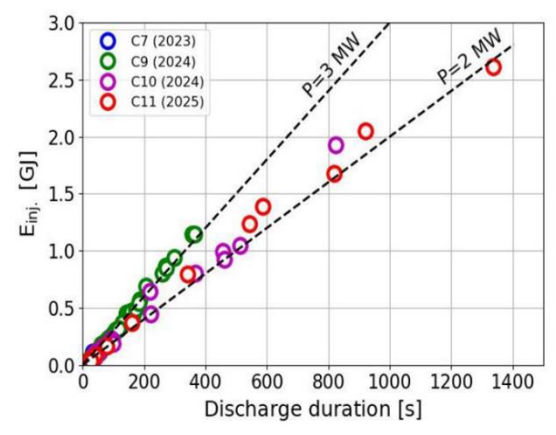


Figure 1: Latest progress in the making of long pulses in WEST. Long pulses beyond 1000s were achieved with less power and lower plasma current.

with more than five hours of plasma each. These results have been made possible thanks to a close monitoring of the campaign, commissioning and shutdown phases with the target of operating the machine during 50% of working days in a year [3]. WEST machine availability of 42% in 2024, reflects the quality-controlled management of maintenance and evolution plans put in place by the operation teams. From this operational experience, several lessons can be drawn for the next step of fusion devices on commissioning of super-conducting coils, technical intervention, actively cooled components protections and diagnostic capabilities for long pulses.

The achievement of long plasma pulses requires key components and systems. Actively cooled PFC must be able to sustain continuous high heat flux up to 10MW/m² on the lower divertor and few MW/m² for on others PFC without causing damage to the material. Therefore, all components inside the vacuum vessel are cooled by a high-pressure (40 bar) and high-temperature (200°C) primary water loop associated to a large cooling circuit network all around the machine. This comprises also the three ICRH antenna and 2 Lower hybrid launchers as well as some of the in-vessel diagnostics (such as endoscopes). These features are essential for long pulse operation and they are all monitored closely by a set of infrared cameras (see below).

In addition, permanent toroidal magnetic field is also required for long plasma pulses. In WEST, it is produced by 18 niobium titanium (NbTi) superconducting winding operated at superfluid temperature 1.8K, encapsulated in thick casings cooled with supercritical helium at 4.5K. The coils have been operated continuously in a reliable way during experimental campaigns.

The study of down-times recorded during experimental campaigns, has shown four main elements/systems impacting WEST operation: the poloidal field, the water and air leaks in vacuum vessel, the CODAC (Control, Data Access and Communication) system and the cryogenic system. Key lessons for future fusion devices have been drawn and now include robust water leak detection and management for actively cooled plasmafacing components, comprehensive thermal protection to prevent damage to uncooled vacuum vessel areas.

Long pulse operation in magnetic fusion devices also requires well controlled plasma power exhaust to the divertor & wall, and avoidance of wall hot spots that could evolve in wall damage (figure 4) [4]. At WEST, 10 major plasma facing components are monitored using 10 series of temperature/power

indicators, based on multiple diagnostic systems, among which the infrared viewing system is especially relevant. These indicators span from the most basic ones to advanced processes using neural networks and machine learning techniques. Some advanced processes do operate in real-time, and feedback on power actuators through the plasma control system providing active control toward remaining within the safe operational domain. Other processes assist with embedded intelligence acquired through machine learning. Some intervene as forensic tools post discharge to identify possible dangerous situation with regard to the power loading to the wall, so that the discharge plan is adjusted to avoid running into potential wall events. No critical wall power event happened during the campaigns C9 to C11 (2024-2025), that would have affected the campaigns operational plan. While it cannot be demonstrated that the active & intelligent wall protection enabled the new plasma duration record of 1337 seconds, it is bound that the wall protection system as a whole helped significantly obtaining this record by preventing wall hot spots to become critical during the campaigns

2.2 Long pulse achievement in 2024 and 2025

With this set-up, WEST has achieved a record pulse length (figure 3) in a full tungsten wall featuring good confinement with H_{98y2} close to unity

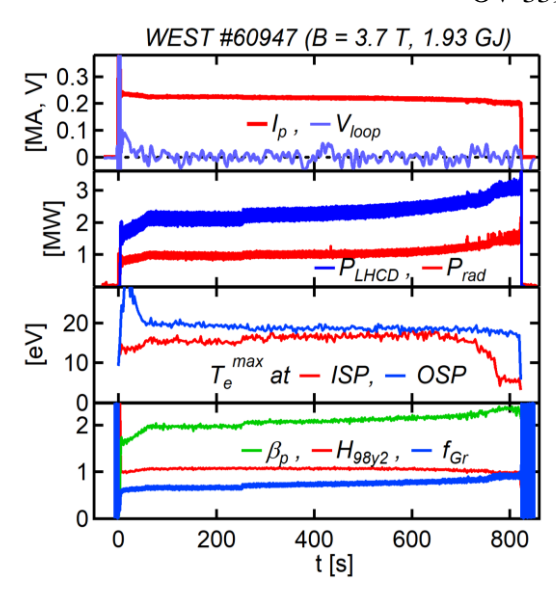


Figure 2: Long pulse of 824s and 1.93GJ of injected energy achieved in WEST in 2024. Note the gradual increase of the density indicating outgassing of in-vessel remote components.

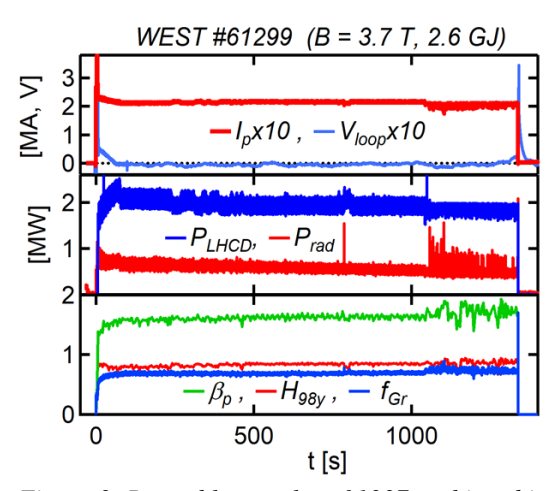


Figure 3: Record long pulse of 1337s achieved in 2025 with 2.6GJ of input energy.

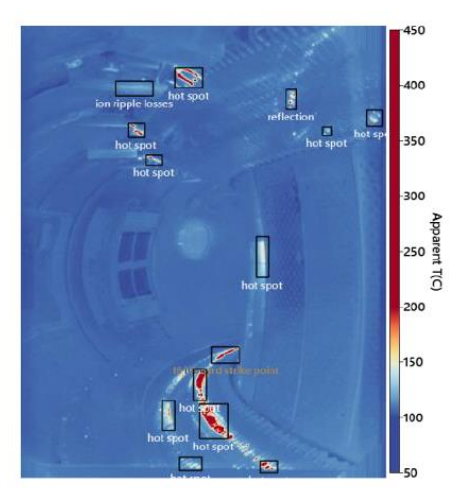


Figure 4: Bounding boxes surrounding thermal events (hot spots) being detected during WEST discharge #60223 by the wide-angle camera and analysed by the wall protection system.

and stationary central electron temperature of ~4keV. For this purpose, the High-Fidelity Plasma Simulator (HFPS), an IMAS version of the JINTRAC/JETTO framework has been used [5]. WEST discharge 57757, lasting 101 s and featuring a loop voltage of Vloop~47 mV has been used as a reference. After a thorough validation, variations in density and plasma current in particular have helped to identify the discharge parameters required to lower V_{loop} until quasi or full non-inductive regime is achieved, while remaining within the boundaries set by physics or operational limits. This extensive simulation effort has resulted in the successful achievements of a large number of non-inductive discharges in WEST during the experimental campaigns carried out between 2023 and 2025 [6]. This is summarized in Figure 1. Twenty discharges have exceeded 200 s. During this effort, several scenarios have been developed. All were based on a double feedback control scheme [7] with a fixed value imposed for V_{loop} by the central solenoid coil voltage, and Ip maintained to its prescribed value by the LH power. On the basis of predictive simulations performed using the HFPS, the first scenarios were performed at Ip~0.27 MA, using a combination of both WEST LH antennas to couple a total power in the range ~3-3.5 MW to the plasma. Figure 2 gives an example of such pulse with a line-averaged central density is $n\bar{l} \sim 3 \times 1019$ m-3. The duration in this case is 810 s with an energy 1.7 GJ. The central electron temperature is Te0~4.3 keV, poloidal beta bp~1.9, normalized toroidal beta $\beta_N \sim 0.9$ and confinement factor H98y2 ~ 1 . In these pulses, density increases progressively throughout the pulse, impacting the LHCD efficiency. This increase is adequately compensated by an increase of the LH power until it becomes significantly more pronounced after t~700 s, inducing a decrease of Ip and a MHD crash. This density increase has been attributed to the outgassing of far-off elements in the vacuum vessel. As a result, new HFPS simulations have been performed to identify parameters with a lower LH power request. It was established that operating at reduced current Ip~0.22 MA and corresponding reduced density n₁~2.4×1019 m-3 would require a LH power in the range 2-2.5 MW. These new discharges do not show outgassing but was terminated by an LH power fault. Technical analysis has shown that these pulses could not have lasted more than ~860 s because of limitations in the capabilities of the RF plant main cooling loop. Remedial measures to overcome this problem was implemented in the last WEST 2025 campaign and new pulses were operated with only the fully-active multi-junction antenna (LH1). This was successful and a pulse of 1337s duration was achieved with an energy injected/extracted reaching 2.61 GJ, a new world record (figure 3). It must be mentioned that pulse 61299 has been run with hydrogen gas, however, several similar pulses used deuterium. A systematic difference between the two classes of pulses (with 2 launchers or with LH1 only) is the presence of mild MHD. This MHD remains mild, the LHCD efficiency does not appear to be severely impacted. On the other hand, the pulses with lower confinement display a mode at frequency ~800 kHz, associated to periodic relaxations of the electron temperature. These relaxations have been analyzed and is characterized by toroidal mode n=1, and poloidal modes m=3 and/or 4. Efforts are ongoing to widen the range of application and increase the performance of the long pulses in WEST by operating at larger densities and using the ECRH power now becoming available in WEST.

3. IMPACT OF LONG PULSE OPERATION ON THE ITER GRADE DIVERTOR OF WEST

WEST provides a testbed for assessing the performance of the ITER divertor under tokamak conditions in advance of ITER operation. In its second phase of operation (phase 2, 2022- present), WEST was equipped with a fully actively cooled tungsten ITER grade divertor, using the same technology (bulk tungsten mono-blocks assembled on a copper heat sink), geometry (featuring in particular a toroidal bevel to protect leading edges as foreseen in ITER, see figure 7a) and thermo-hydraulic conditions (water cooling at 70°C) as planned for ITER [8]. This has enabled the full long pulse capability of WEST, and allowed cumulating more than 18 hours of plasma exposure in phase 2, as well setting new records in pulse duration, as described in section 2. The first part of this section describes the plasma exposure conditions, while the second part details observations of the ITER divertor after plasma exposure.

3.1 Providing relevant divertor heat fluxes and particle fluence in WEST

Steady progress has been made in WEST for providing ITER relevant steady state heat fluxes. Figure 5 shows the peak divertor heat flux reached at the outer strike point as a function of the power entering the scrape off layer (SOL). Heat fluxes in the range foreseen for ITER (5-10 MW/m², see [10]) are routinely achieved, while heat fluxes above the nominal ITER specification of 10 MW/m² were reached for dedicated divertor testing experiments (such as mono-block melting experiments [11]). The first high fluence

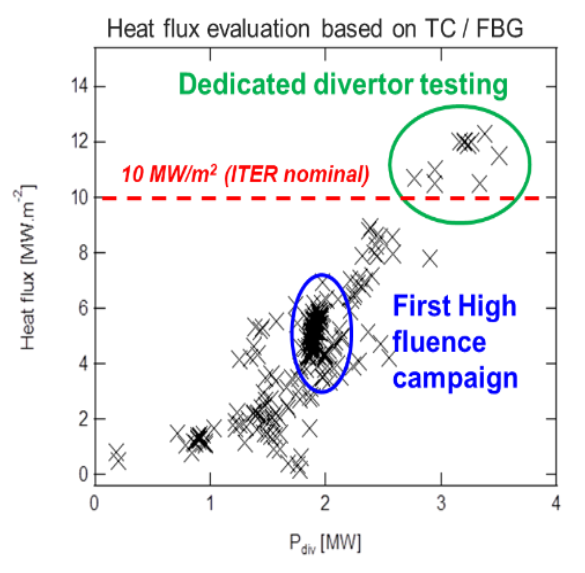


Figure 5: Peak divertor heat, as measured by thermal embedded diagnostics (Fiber Bragg Gratings (FBG), thermocouples (TC), see [9] for the methodology used) flux as a function of the power entering the SOL (total power minus the power radiated in the confined plasma). The database shown includes only data where the thermal equilibrium of the divertor was reached (typically for pulses with a phase where additional power was applied for > 5s)

campaign of WEST, using repetitive pulses of 60s to cumulate significant divertor particle fluence, was performed under heat fluxes of the order of 5 MW/m² [12]. It should be outlined that WEST was successfully designed for reaching significant divertor heat fluxes using moderate additional power. Finally, in addition to steady state heat fluxes, the divertor was loaded with a significant number of transients (> 2400 disruptions over phase 2), although WEST was operated in L mode so far.

In terms of divertor particle fluence, WEST has now cumulated more than 1.7 10^{27} D/m² in the outer strike point area, as shown in figure 6. This would correspond to a few ITER Q=10 400s nominal shots. Most plasma were run under attached divertor conditions prone to tungsten erosion by intrinsic impurities, with T_e in the range 20-40 eV. Roughly 10% of the pulses were performed under cold divertor conditions in the last campaigns (C10-C11), mitigating tungsten erosion, with T_e < 10 eV. This is the case for the X Point Radiator scenario (XPR), detailed in section 4.

3.2 Evolution of the ITER grade divertor under WEST phase 2 plasma exposure

Crack networks were observed on the top surface of the bevelled mono-blocks of the ITER grade divertor

x1027

1.75

1.75

1.50

1.50

1.50

1.50

1.5MA 400s

ITER pulse

Figure 6: Divertor particle fluence cumulated over the experimental campaigns of WEST during phase 2(campaign C7 to C11), measured by divertor Langmuir probes, as a function of mono-blocks (MB) position along the divertor (MB1 corresponds to the high field side, MB 34 to the low field side). Typical positions for the inner strike point (ISP, MB14-18) and the outer strike point (OSP, MB24-MB28) are also indicated. The dedicated high fluence campaign is shown in dark blue. Typical peak divertor fluence expected for an ITER nominal shot (Q=10, 15 MA, 400s) is also indicated for comparison.

after the first campaign of phase 2 [13, 14], although the divertor was exposed to mild steady state heat fluxes (in the range 5-10 MW/m²), where tungsten cracking would not be expected based on results from testing in high heat flux facilities. Cracks were observed in the plasma wetted surface of the outer strike point area (on MB 26-28, with most pronounced cracking on MB27), as shown in Figure 7b. Those cracks were also visible in operando with the Very High-Resolution infrared (VHR IR) camera of WEST [15], as illustrated in Figure 7b. This observation is in contrast with unbevelled monoblocks exposed in the phase 1 of WEST, where cracks and local melting were observed on the exposed leading edges, both in the inner and outer strike points area, in particular for misaligned components [16]. This was explained by the impact of disruptions on "cold" mono-blocks, with simulations showing that conditions for crack formation were met during the post disruption cooling phase [17]. The observations from phase 2 exposure confirm that the toroidal bevel protects leading edges as expected (see figure 7a) for an illustration). However, although cracks on the top surface were to be expected under the harsh conditions of ITER (in particular for disruptions or unmitigated ELMs), they were not anticipated under the milder loading conditions in WEST. In order to investigate the cause for crack formation, dedicated tests in the high heat flux facility HADES [18] were performed on pristine MB, in conditions mimicking WEST exposure in terms of disruption heat loading on the top surface of cold or heated MB. In particular, heat loads were concentrated on the part of

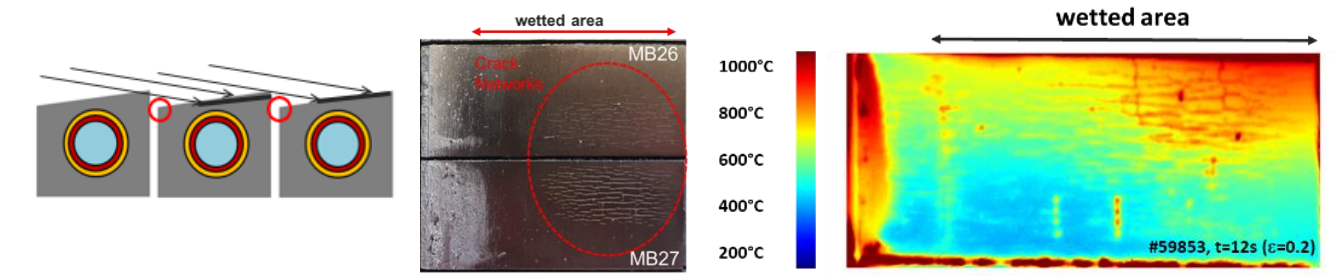


Figure 7a. (left) Schematic view of mono-blocks (MB) featuring a toroidal bevel protecting the leading edges (circled in red). Magnetic field lines are shown to illustrate the plasma shadowed and the plasma wetted area of the MB (exaggerated angle of incidence for the sake of the illustration).

Figure 7b (middle): view of the top surface of 2 MB exposed in the strike point area of WEST, featuring crack network in the area exposed to the plasma.

Figure 7c (right): view of one MB in WEST with the Very High-Resolution infrared camera, able to discriminate cracks during operation.

the MB corresponding to the plasma wetted area in WEST (~75% of the MB surface) to reproduce the thermal gradients developing in actively cooled components under tokamak conditions (see figure 1-b in [14]). However, the highly peaked steady state heat flux deposition in the plasma wetted area, due to the narrow heat SOL width in tokamak conditions, could not be reproduced in HADES. The tests in HADES did not reveal any cracking, even under the most severe conditions tested, underlining the difficulty of reproducing tokamak conditions in HHF facilities and the potential impact of deuterium

loading on the thermo-mechanical behaviour of plasma facing components. Further numerical and experimental studies are required to understand the damage mechanism at play. The crack network is still present on the divertor MB top surface after several experimental campaigns of WEST phase 2, but did not hamper their heat exhaust capabilities so far.

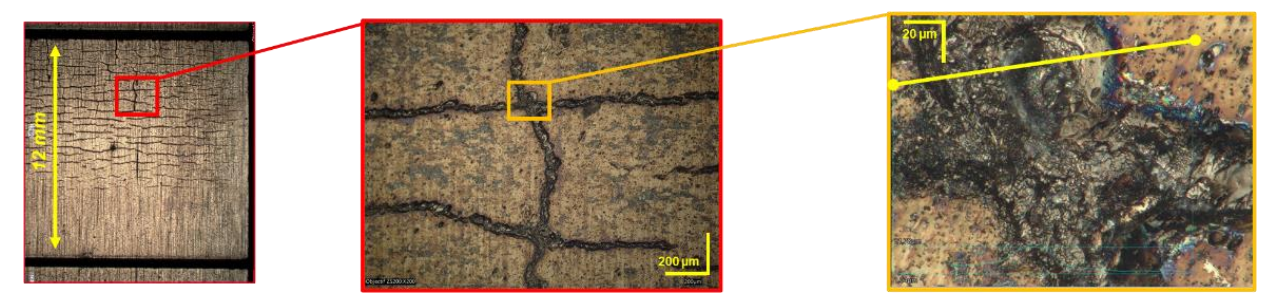


Figure 8: Progressive zoom (from left to right) on the top surface of a MB exposed in the outer strike point area of WEST (PFU 357-MB27) after the C11 campaign, showing how cracks are being filled up with molten material. The yellow line on the right-hand side graph shows where the post mortem analysis was made to characterize the ridge at the crack position.

The most recent observations after the last experimental campaign (C11) reveal that cracks are being filled up by molten material, bridging the cracks and creating ridges of more than 10 microns of height above the surface (figure 8).

The WEST divertor also exhibits a pronounced erosion / deposition pattern after 18 hours of plasma exposure in phase 2, as illustrated in figure 9 [13,19]. Net erosion is found in the strike points area (both inner and outer), with erosion up to ~25 microns. This corresponds to a campaign integrated net erosion rate in the range 0.1-0.5 nm/s, in the same range as found in AUG, although under different plasma exposure conditions. Such a net erosion rate would be marginally acceptable in terms of divertor lifetime for the 700 hours of plasma exposure expected in the DT-1 phase of ITER [20], although nominal plasma conditions in ITER (semi-detached divertor conditions) are expected to be far less prone to W erosion.

Significant deposition, with deposited layers building up to 300 microns after the C11 campaign (18 hours of plasma exposure), is also found on the inner divertor, with a sharp transition between the erosion and the deposition dominated area ([13,19]). This is reminiscent of observations in other tokamaks, with deposited layers building up on the high field side (HFS) of the divertor [21, 22]. In the case of WEST, those HFS deposited layers were shown to be prone to flaking during operation, leading to impurity ingress in the plasma (so called "UFO"). This was observed for the first time during the first high fluence campaign (C7 campaign), where 1/3 of the plasma attempts were hampered by UFO by the end of the campaign [12]. This led to developing cleaning procedures for removing deposited layers, first partial cleaning performed manually between campaigns, then a fully efficient laser cleaning performed for the first time during the summer shutdown of 2025. This is further detailed in the following paragraph. The evolution of the erosion / deposition pattern on the ITER grade divertor of WEST and the consequences in terms of plasma operation shows that it is important to minimize erosion, but also deposition when running long pulses.

When running repetitive long pulses in high fluence campaign, an increasing number of radiative events is observed, becoming

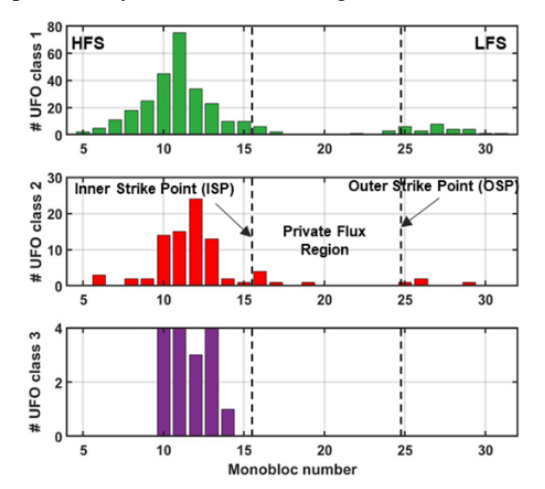
MB number 10 15 20 25 30 35 40 5 (<u>F</u> 400 350 300 250 OSP 200 ₹ 150 100 50 0 -50 0 100 200 300 400 500 s coordinate (mm)

Figure 9: Net erosion / deposition profile along the WEST ITER grade divertor after the C11 campaign (18 hours of plasma exposure), estimated from confocal microscopy. Data shown correspond to area of maximum erosion/deposition in the global pattern modulated by the ripple. Areas of net erosion are shown in yellow (corresponding to the inner and outer strike point area) while the area of thick deposition is shown in blue. The other areas (where no data are shown) correspond to thin deposits [11, 17]. The red dots correspond to areas where no cleaning was applied to investigate the deposited layers build up, while the blue dots correspond to areas which were partially cleaned between campaigns.

significant once the cumulated injected energy reached ~20GJ [23]. Usually, they only have transient impact on the radiated power and other plasma quantities. Using the 6 infrared Divertor views available (85% divertor coverage), the 5 antenna views and the wide-angle camera, UFO localization and size could be characterized. They have been categorized in 3 different class: Class 1 is « benign impact » UFOs: the plasma survives without subsequent issues; Class 2 dubbed « medium impact » UFOs: bifurcation into the cold branch regime prone to MHD activity and finally disruption with delay >200ms; and Class 3 « large impact » UFO: leading to fast disruption in less than 200ms. The UFO originate mostly from the inner maximum heat flux area on the high field side which is a thick deposit area as described above. During the high fluence campaign with cumulated operation of ~5 hours representative of a few ITER pulses, UFOs are constantly increased in frequency starting with class 1 UFOs and then more and more class 2 and class 3 occurred (figure 10a and 10b). The fast occurrence of the UFO class 1 is likely due to layers accumulated on the divertor from the previous plasma experiments performed before the start of the high fluence campaign. From the plasma response analysis (radiated power, Zeff), UFO

are thought to be mainly composed of W. In total, the cumulated W mass in UFOs is estimated around 15mg of W after a fluence of 5.10^{26} part/m².

In order to avoid further perturbation on plasma operation due to UFO, a procedure was developed to remove deposited layers without altering the W substrate. Based on recent development in cleaning processes using laser in



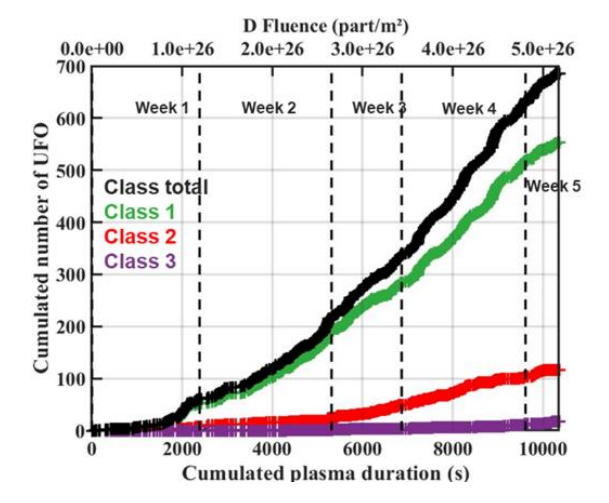


Figure 10a (left): number of UFOs detected by their provenance (monobloc from high field side to low field side). From top to bottom: green=benign UFOs, red=UFOs leading to high radiation and eventually to disruption, purple=immediate disruption.

Figure 10b (right): Cumulated number of UFOs observed in a high fluence campaign for each class of UFOs.

industry, a method was devised to fully recover the W substrate (figure 11) [24]. It relies on the generation of a plasma which induces thermo-mechanical stress on the deposited layer and breaks the deposit interface. Vapors and dusts are extracted near the plasma formation thus avoiding material redeposition. A 1064nm pulsed fiber laser with 1mJ energy has been chosen. The laser gaussian profile has a pulse length of 150ns and the laser is pulsed with a frequency of 100Hz. Frequency and energy had been adjusted in order to exclude any alteration of the W surface while creating a plasma that vaporize and ablate the deposit. This new process had been successfully applied during the summer 2025 shutdown on the entire lower divertor, including both out of the vessel (1/4 of the sectors) and in vessel operations (3/4 of the sectors). In total, the removed deposit weight is about 190g for the whole divertor.

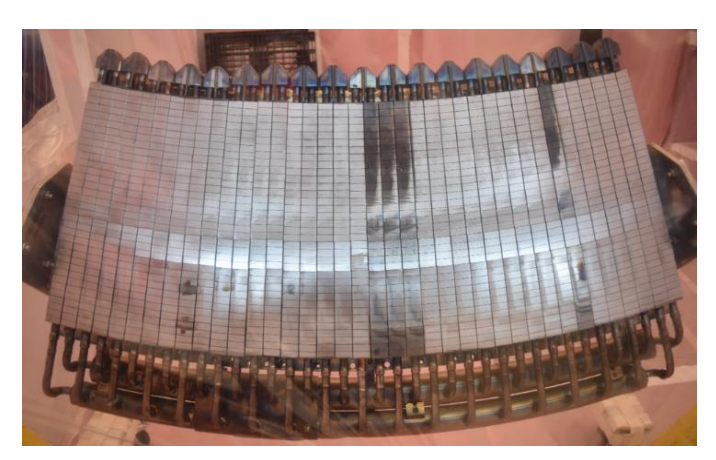


Figure 11: element of the divertor plate cleaned up by the laser technique. Note the 4 unclean PFUs that have been left uncleaned as reference

4. PLASMA EXHAUST SCENARIO FOR LIMITING EROSION (XPR)

In 2023, experiments performed with nitrogen seeding reported that the W divertor sources can be extinguished and create a transition to a so-called X-point Radiator (XPR) regime similar to earlier results from AUG [25]. In WEST, XPR regimes are produced by injection of nitrogen in L-mode scenarios. They have been found to be stable and controllable over a range of density (ne) ~ 2.5 – 4.5 m-2, input power from PIN ~ 0.5 (ohmic) to 5 MW, and plasma currents from 250 to 500 kA. Upon sufficient seeding, the WEST divertor plasma, which is initially hot ("attached plasma") with electron temperatures in the 20 to 40 eV range, eventually transitions into a cold (< 3 eV) and dense ($n_e \sim 8-10 \times 10^{19}$ m⁻³) plasma at the divertor targets, with mitigated heat loads by factors of ~10, but with still finite ion flux to the divertor targets [26]. This condensation of the divertor plasma coincides with the appearance of the characteristic stable toroidal radiation ring (MARFE like) just above the X-Point, from where the name "X-Point Radiator" is derived. A record XPR phase of 34s was also achieved (figure 12 and 13) using real time control of the line average density crossing the X-point as an observer of the dense region above the X-point dense ($n_e \sim 8-10 \times 10^{19}$ m-3). This forms now the basis for testing the WEST divertor ITER-grade plasma facing components (PFC) in more ITER relevant conditions: i.e., at high particle fluence and sub-10 eV temperatures (vs. high particle fluence at Te > 20 eV in previous high fluence campaigns).

It is observed that the time traces of the temperature from Langmuir probe measurements at the inner and outer strike

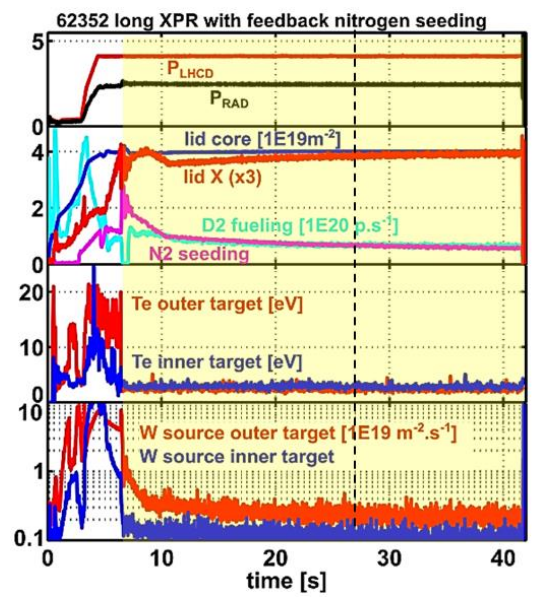


Figure 12: Longest XPR phase of 34s achieved in 2025 in WEST in 2025. Note the low level of tungsten sources on both outer and inner targets.



Figure 13: Visible camera view of discharge 62352 at 27s. Note the presence of the MARFE in the X-point area and the N2 injection.

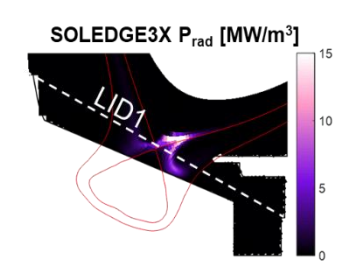


Figure 14: modelling of the radiated power during the XPR including drifts. The dashed line represents the interferometry channel (LID1) across the X-point used for real time control of nitrogen during the experiment.

points are not evolving in the same way. When the XPR occurs the outer target electron temperature undergoes an abrupt decrease to 3-5 eV. This so-called "Te cliff" has a very short time scale and the drop in electron temperature occurs within a few microseconds.

In the last 2 years, the study of exhaust physics with the long pulse X point radiator regime has been extended to different plasma

magnetic configurations (double null and upper/lower single null) revealing the importance of drifts. Indeed, attempts to trigger such regimes in Upper-Single Null (USN), which corresponds to the "unfavorable" configuration in WEST, leads to different behaviors. This highlights the importance of the direction of drift flows to accurately describe the transition dynamics and stability in XPR scenarios. Since flows (and thus also drift flows) are also of high importance in material erosion, contamination and migration/redeposition matters, boundary simulations with the SOLEDGE3X code have included the drift for describing the radiation map at the X-point (figure 14) [27].

Core plasma performance improves upon nitrogen injection with significant increases of core confinement (τ_E +25%, from ion dilution effects), central Te (+20%), and Ti (+35%) [28], and those benefits remain through the transition to the XPR state. Such improvements are simultaneous with the reduced W contamination from tamed divertor sources. At the same time a significant enhancement of the edge rotation is observed from Doppler Back Scattering measurements [27].

A new ion temperature measurement from the retarding field analyser located on the divertor target (figure 15) [29] has revealed a strong dependence of the ion temperature with the dissipation regime (detached or attached). In case of the conventional attached scenario the ion temperature is much higher (by a factor 3 to 6) than the electron temperature. In case of detached plasma, the ion temperature drops to about the same level as the electron temperature. Such high ion temperature in conventional scenario is consistent with the heat flux along the field lines reconstruction from the high-resolution infrared camera and embedded divertor thermal diagnostics.

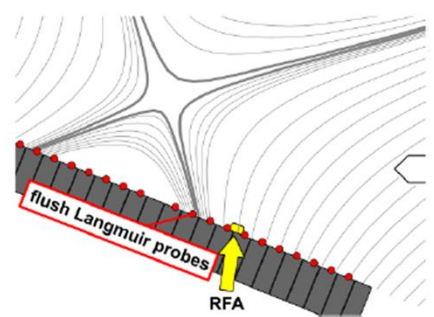


Figure 15: retarding field amplifier probe measuring the ion temperature on the target plate.

5. ADDITIONAL CONTRIBUTION TO THE ITER BASELINE

5.1 Plasma restart and boronization

A central question for ITER-relevant operation is whether a device with a full-W wall can reliably restart after a vent without glow discharge boronization (GDB). Toroidally non-uniform GDB is investigated [30] and modelled [31] since ITER will have a non-uniform toroidal distribution of the glow anodes in the first phase of the machine (SRO) [32]. WEST has therefore executed a controlled plasma restart programme with limiter ohmic pulses (without ECRH) on newly installed bulk-W inboard tiles, before and after deliberately non-uniform GDB. WEST is equipped with six glow anodes and six toroidal B2D6 injection points [33]; for this experiment, all six anodes were energized but only three of the six injection locations were

60496 / 60527: before / after boronization

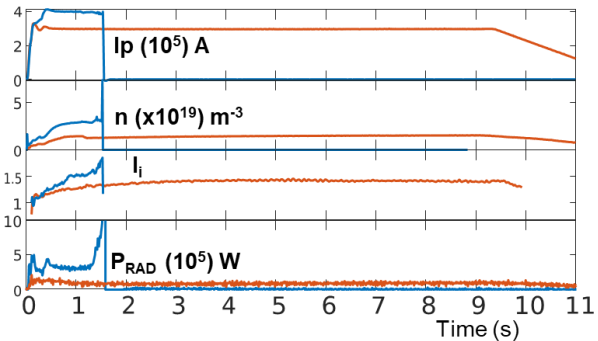
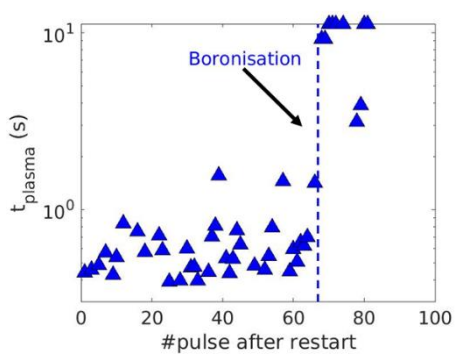


Figure 16: Comparison of two discharges start-up before (blue) and after GDB (red), the last one up to the end.

used. The sequence comprised (i) repeated restart attempts without GDB, (ii) application of the non-uniform GDB, and (iii) identical restart attempts. The operational figure of merit was to reach the requested 10 s pulse length with reproducibility over consecutive shots. Before GDB, only a few plasmas exceeded 1 s; many attempts terminated radiatively, showed high internal inductance (figure 16) and stalled early despite modest shot-to-shot improvement. Immediately after the non-uniform GDB (right of the divider on figure 17a), the same operating scenario requests produced plasmas lasting more than tens of seconds from the outset [33]. These results are comparable to those reported by the ASDEX Upgrade team [34]. This experiment confirms that GDB is likely to become instrumental in plasma restart in the new full tungsten wall configuration of ITER.

In addition, probe equipped with samples were introduced in the vessel during the non-uniform GDB [35]. These probes (figure 17b) were exposed to the glow discharge GDB in two different toroidal location (figure), close and away from the B2D6 injection points. Preliminary analysis of the probes indicates that the probes far from the injection do receive B although less than the probes located near the injection and even if B deposition is lower away from injection points, the asymmetry is not larger than 40%.

However, the recent modelling for WEST based on Monte Carlo simulations of diborane molecules glow





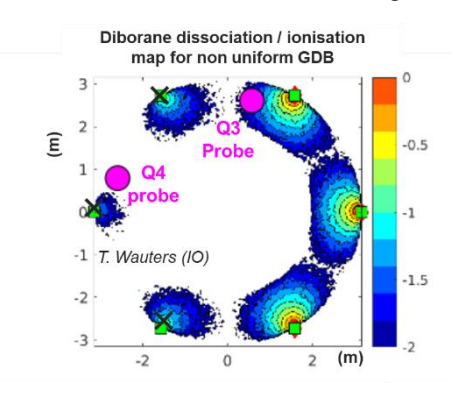


Figure 17a (left): plasma duration before and after GDB.

Figure 17b (middle): photograph of the probe carrying the samples (white squares) exposed to glow discharge with boron.

Figure 17c (right): toroidal view of the modelling of the diborane dissociation map for WEST. Pink dots are toroidal locations of the probe samples in WEST. Green square are the locations of diborane injections. Only 3 out of 6 were

discharge plasma [31] indicated that a non-uniform GDB (which is the configuration in the Start of Research Operations phase of ITER) would not be able to deposit B on surfaces far from the injection (figure 17c). The contrasting experimental results from WEST are therefore providing new insights in the modelling of GDB for ITER.

The second potential issue related to the use of GDB is linked with fuel retention. Relative to the pre-GDB discharges, the first post-GDB shots seem show higher retention, consistent with additional trapping sites in the freshly boronised surface. As cumulative exposure increases across the seven post-GDB ohmic shots (identical scenario), the retention decreases towards the pre-GDB level after 4 or 5 pulses [36], but more experiments are still needed to quantify this effect.

Regarding the use of boron, the impact of injecting Boron particulates with the Impurity Powder Dropper (IPD)on the discharge properties (confinement, impurity transport etc.) has also been analyzed in WEST [37]. First Ion Cyclotron Wall Conditioning (ICWC) experiments has also taken place in WEST as an alternative conditioning method for ITER.

5.2 Modelling of isotopic change over for ITER grades components.

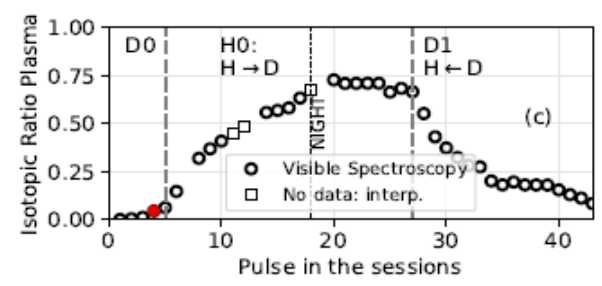
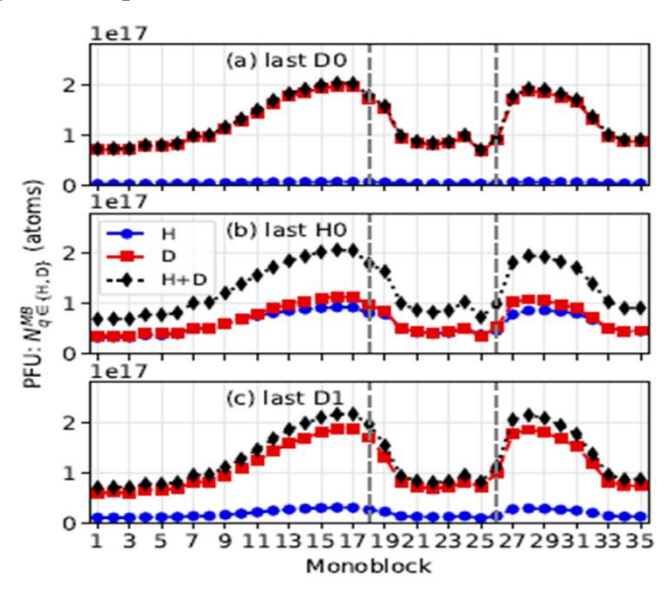


Figure 18a (above): Isotopic ratio measured by visible spectroscopy for the sequence of discharges operated during the changeover starting with deuterium, then D to H and finally H to D.

Figure 18b (right): H, D and total (H+D) inventory along a PFU for each mono-block for the last pulse of each phase: D0 (a), H0 (b) and D1 (c). The gray vertical dashed lines show the position of the maximum inner and outer heat fluxes.



Modelling of D/H retention in the WEST divertor was performed with the MHIMS code for a D/H/D changeover experiment [38] figure 18a. Model was validated using laboratory experiments and the partial pressure decay at the end of the changeover. During the H-plasma phase, the H2 dynamic is similar in the experiment and simulation but during the D-plasma phase, there is a small source of H2 outgassing increasing the partial pressure of H2 which has not been included in the simulation (figure 18b). After the last D-plasma of the following D-plasma phase: the surface is again dominated by D but there is a remain of H content deep in the bulk (seen by the rise of the isotopic ratio around 200 μ m). Retention pattern are very dependent on heat flux exposure conditions. The isotopic exchange is limited by the migration of the exposed species in the bulk: the longer the cleaning pulse are, the more fuel can be recovered. The isotope exchange is fast near the material surface but limited deeper due to slow hydrogen transport in the material. The analysis also indicates that the changeover is an efficient tool to recover hydrogen isotopes in the plasma-exposed near surface (up to 100μ m), but not enough to reach D trapped deeper in the material. Positioning the strike point at the position of the maximum retention could enhanced the isotopic exchange by increasing the temperature and speeding up the hydrogen transport similarly to the raised inner/outer strike point tested in JET [39].

5.3 Run-away mitigation and impact studies

For the first time, WEST has recently produced reliable runaway electron (RE) beam scenario with plasma current up to 650 kA and lasting 0.3s to 1.2s. These runaway beams were generated with a large pre-disruption seed using argon gas. Once the runaway beam was created, D_2 was injected (figure 19) to test benign RE termination schemes. This led to the recombination of the cold companion plasma coexisting with the runaway beam. When the runaways were ultimately lost, a "benign termination" ensued, with no damage on the plasma facing components, as observed on other tokamaks. These experiments benefited from the monitoring of a whole set of newly installed diagnostics such as REIS [40], fast multispectral IR camera, X-rays, fast visible camera. The measurements will help understanding the limits and the extrapolability of this termination scenario to future tokamaks [41]

In addition, a controlled RE damage experiment was achieved in WEST by controlling and landing a RE beam on an instrumented tile of the tungsten inner wall (figure 20a, 20b and 20c). The RE crash was fully diagnosed with fast & IR visible camera,

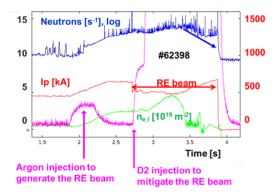


Figure 19: Run-away mitigation in WEST. Note the decay of the neutron (blue) and the increase of the plasma current (red) as the plasma recombines after the D2 injection at

REIS and Langmuir probes, as well as the thermocouples embedded in the instrumented tile [14, 40]. The runaway beam lasted 0.54s and it could be determined that the average energy of the electrons was in the range of 15 to 17MeV with a pitch angle of 0.3rad. The crash occurred in a very short time (2.5ms). These data form now the basis for validating the complex workflow used for modelling RE damage in typical ITER tungsten components. Post mortem analysis is also in progress.

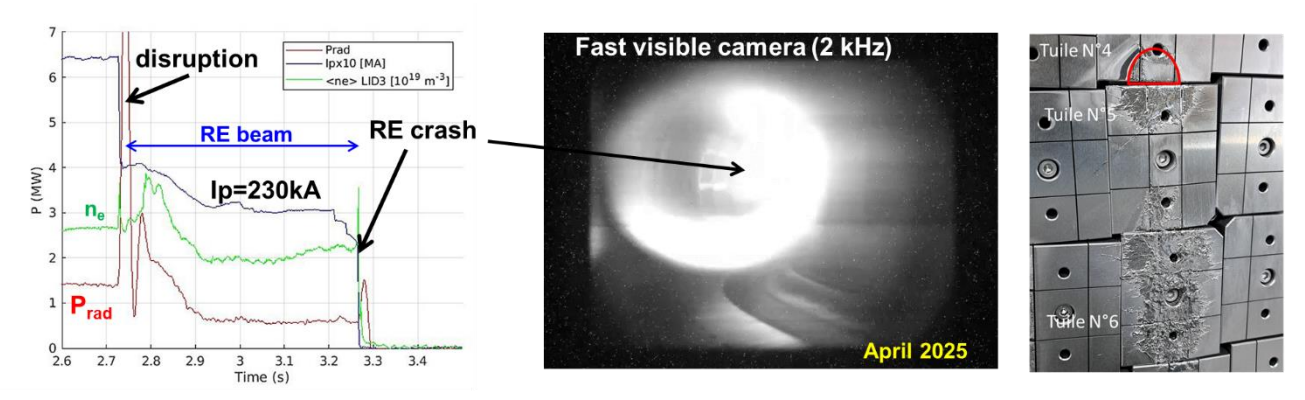


Figure 20a (left): Time traces of the intentional run-away crash operated in WEST on an inner wall tungsten tile. Figure 20b (middle): camera view of the crash.

Figure 20c (right): photograph of the impact on the inner wall tile $N^{\circ}6$.

5.4 Recent modelling advances

Estimating edge plasma turbulent transport remains a significant challenge for numerical modelling. Various approaches have been developed within the community, each offering distinct levels of predictive capability and computational cost. For this objective, the SOLEDGE3X code developed at CEA/IRFM [43], implements three different approaches. The first approach uses rapid mean-field transport solvers often employing ad hoc empirical diffusivities to

reproduce experimental observations (low predictability, good experimental agreement, computationally inexpensive). In contrast, the second approach addresses first-principles three-dimensional turbulence simulations which although considerably more computationally demanding, are not relying on experimental inputs and can achieve reasonable consistency with experimental results when multi-physics effects such as neutrals and impurities are included (high predictability, fair experimental agreement, computationally expensive). Between these two extremes approaches, emerging strategies based on reduced turbulence models seek to incorporate essential turbulence physics into mean-field simulations, thereby improving predictive capability while maintaining manageable computational requirements (good predictability, fair experimental agreement, moderate cost). All three approaches have been confronted to data from TCV experiments and are showing that depending of the purpose (experiment, interpretation, prediction, ...), they can be used efficiently [44]

In addition, recent experiments in WEST and other devices [45] as well as numerical simulations have revived past observations highlighting the beneficial role for plasma confinement of magnetic equilibria with negative triangularity (NT). From the theoretical point of view, the reasons for such an improvement remain unclear. A reduced model for trapped electron mode stability has been developed, which incorporates the basic effects of elongation and triangularity [46]. The key findings are twofold: NT usually leads to linearly more unstable TEM, unless finite mode extent (ballooning) and – to a less extent – finite orbit width is accounted for. These effects give more weight to particles trapped at low bounce angles, which are those that exhibit lower precession frequencies at NT compared to PT.

In the L-mode plasmas of Tore Supra and WEST tokamaks, it is observed that the well of the radial electric field Er near the separatrix is observed to deepen when the safety factor decreases [47]. This observation is of importance in view of optimizing the onset of the H-mode on WEST. Flux-driven simulations of ion temperature gradient turbulence with GYSELA recover qualitatively this trend and point towards the following mechanism [48]. Turbulence plays a key role in the establishment of Er at the edge [49]. Although the turbulent drive of Er – the Reynolds stress – is reduced at low q (consistently with lower turbulence at large plasma current), it turns out that the damping of this poloidal flow governed by neoclassical physics is reduced even more strongly, resulting in an overall increase of the magnitude of Er when q decreases.

6. CONCLUSIONS AND OUTLOOK

In the past 2 years WEST has developed long pulses operation on a routine basis and tested ITER grade components with particle fluence and heat load approaching those of ITER. ITER grade components have been tested up to 12MW/m2 and cracks have been observed on the mono-block exposed top surface. Cracks do not seem to hamper the divertor heat exhaust capability and do not cause operation consequences. After extensive plasma exposure in phase 2, analyses show a net erosion of 0.1 to 0.5nm/s at the strike point, and a redeposition area on the high field side which generates UFO hampering plasma operation. The XPR detached regime of operation has been extended to 34s using real time control and physics understanding has been gained using SOLEDGE including drifts. This scenario will be further developed to even longer pulses for carrying out high fluence campaign in cold divertor conditions. In support of the ITER baseline, non-uniform GDB has been tested in WEST and is efficient for plasma start-up. In contrast to preliminary modelling, non-uniform GCB has an impact away from the diborane injection points. New run-away experiments (up to 0.5s of RE beam) confirms RE mitigation by D2 injection and is now addressing component damage in support of ITER.

In the next two years, WEST will carry on operating long pulse assisted with an additional ECRH power of up to 3MW which is essential for mastering current profile, tungsten transport and getting into a stable H-mode regime.

The ongoing installation of a 3MW Electron Cyclotron Resonant Heating (ECRH) system at frequency 105GHz [50] will expand WEST plasma scenarios and allow transition to the H-mode phase. Integrated modelling confirms that this additional power source can be instrumental in opening the operational space of WEST [6].

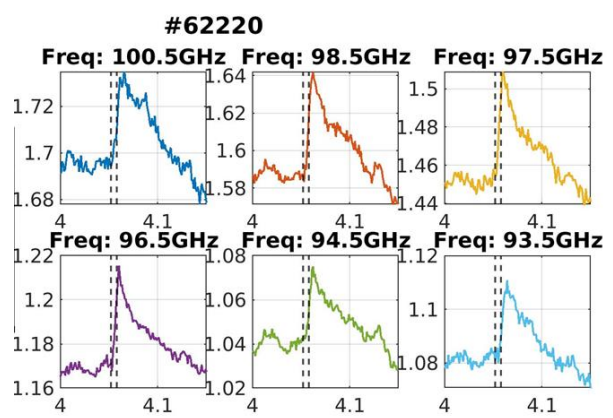


Figure 21: Signals of 6 ECE channels showing the first ECRH power coupled to a WEST plasma at 4.05s.

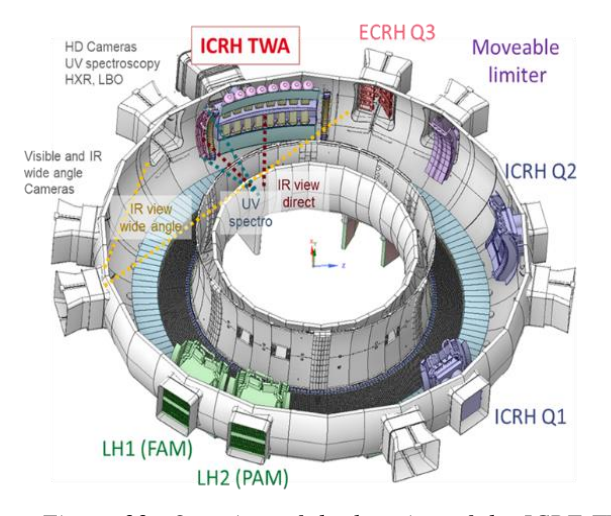


Figure 22: Overview of the location of the ICRF TWA launchers in the WEST tokamak. The fields of view of the infra-red camera monitoring the TWA launchers are illustrated in yellow as well as the visible spectroscopy lines related to the left side limiter.

3 gyrotrons with performance of 1MW/1000s per unit are planned. The first gyrotron has been commissioned and coupled to the plasma (figure 21). The THALES company will deliver two additional gyrotrons: 2 MW will be available in April 2026 and the WEST ECRH system will reach an EC power of 3 MW by the end of 2026. The injected energy will be limited in 2026 by the launcher and transmission line components, which will be upgraded in the near future.

A Travelling Wave Array (TWA) system for Ion Cyclotron Range of Frequency (ICRF) is currently under design for the WEST facility in collaboration wth LPP-ERM-KMS, DTU and ASIPP [51]. This system aims to address the limitations of current ICRF resonant launchers, focusing on improved coupling, reduced voltages and RF sheaths [2], and enhanced reliability. The goal of the TWA project is to test two TWA ICRF launchers on WEST plasmas. Figure 22 shows an overview of the relevant WEST internal components, with the two TWA launchers located next to the ECRH launcher. The TWA ICRF launchers will replace one existing ICRF launcher located in the Q4 port. As WEST is a superconducting machine running long plasma pulses, the launchers will be actively cooled.

The future experimental program associated with the operation of the TWA launchers in WEST includes a comprehensive set of experiments to characterize the performance and capabilities of this new system. First, the coupling properties of the launchers will be characterized for various plasma shapes and distances, along with the system heating efficiency. As the launchers are wide-band, it will be possible to change the RF frequency during plasma operation in real-time, opening a new operational domain, for example, for turbulence control.

In the longer term, beyond 2027, WEST is planning to increase its long pulse and heat load handling capabilities by replacing the present set of W limiters with recessed stainless-steel panels with full tungsten first wall (figure 23a, 23b and 23c) [52]. This will enable the machine to operate long pulses at a higher injected power per surface unit, thus reaching high power exhaust over ITER relevant pulse duration. With this new set-up WEST will be in a position to contribute decisively to the first phase of ITER.

WEST Phase 2 (now)



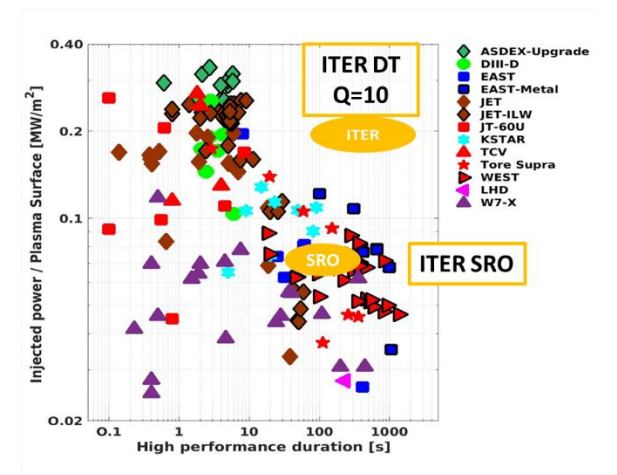




Figure 23a (left): present in-vessel configuration of WEST made of stainless-steel water-cooled panels. The present WEST operation corresponds to the ITER SRO domain (orange patch) in figure 23b.

Figure 23b (right): injected power per plasma surface unit as function of the pulse length. With more injected power, WEST could reach high power exhaust near the range of ITER.

Figure 23c (right): New proposed tungsten arrangement of the inner tungsten wall. The future WEST operation corresponds to the ITER DT Q=10 orange patch in figure 23b.

7. ACKNOWLEDGEMENTS

This work has been carried out within the framework of the EUROfusion Consortium, funded by the European Union via the Euratom Research and Training Programme (Grant Agreement No 101052200 — EUROfusion). Views and opinions expressed are however those of the author(s) only and do not necessarily reflect those of the European Union or the European Commission. Neither the European Union nor the European Commission can be held responsible for them.

8. REFERENCE

- [1] P. Barabaschi et al., this conference OV-2303
- [2] J. Bucalossi et al, Nucl. Fusion 64 (2024) 112022
- [3] V. Lamaison et al, this conference, TEC-FNT 2927
- [4] R. Mitteau et al, this conference, TEC-IVC 3049
- [5] T. Fonghetti et al., WEST L-mode record long pulses guided by predictions using Integrated Modeling, Nucl. Fusion 65 5 (2025) 056018.
- [6] R. Dumont et al, this conference, EX-C 2904
- [7] R. Noualleitas et al., Fusion Engineering Design, Volume 59, Issue 11, 2025, Pages 186-191
- [8] M. Missirlian et al., Fusion Engineering and Design, Volume 193, August 2023, 113683
- [9] Y. Anquetin et al., Nuclear Materials and Energy, Volume 41, December 2024, 101788

- [10] R. Pitts, et al., Nuclear Materials and Energy, Volume 20, August 2019, 100696
- [11] Y Corre et al 2021 Phys. Scr. 96 124057
- [12] J. Gaspar et al., Nuclear Materials and Energy, Volume 41, December 2024, 101745
- [13] M. Diez et al., 20th International Conference on Plasma-Facing Materials and Components for Fusion Applications, Ljubljana, Slovenia, 19–23 May 2025
- [14] Y. Corre et al., this conference EX-M 2938
- [15] M. H Aumenier et al., Nuclear Materials and Energy, Volume 26, March 2021, 100879
- [16] M. Diez et al 2021 Nucl. Fusion 61 106011
- [17] A. Durif, et al., Fusion Engineering and Design, Volume 188, March 2023, 113441 Reference HADES
- [18] H. Roche et al., Fusion Engineering and Design, Volume 192, July 2023, 113769
- [19] A. Hakola et al., this conference, EX-M 2788
- [20] T. Wauters et al., 20th International Conference on Plasma-Facing Materials and Components for Fusion Applications, Ljubljana, Slovenia, 19–23 May 2025.
- [21] Anna Widdowson et al 2021 Phys. Scr. 96 124075
- [22] A. Hakola et al., Nuclear Materials and Energy, Volume 12, August 2017, Pages 423-428
- [23] J. Gaspar et al, NME 41 (2024) 101783
- [24] M. Firdaouss et al., ICFRM 22, 29 September 3 October 2025 Shizuoaka, Japon to be published in NME
- [25] M. Bernert et al., Nuclear Materials and Energy, Volume 34, March 2023, 101376
- [26] N. Rivals et al., Nuc. Mater. Energy 40 (2025) 101723
- [27] N. Rivals, this conference EX-D 3067
- [28] P. Forestier-Colleoni et al. submitted to Nucl. Fus., 2025
- [29] P. Ivanova, J. Gunn et al., to be submitted to Plasma Physics and Controlled Fusion, 2025.
- [30] A. Gallo et al., 20th International Conference on Plasma-Facing Materials and Components for Fusion Applications, Ljubljana, Slovenia, 19–23 May 2025
- [31] T. Wauters et al., Nuclear Materials and Energy, Volume 42, March 2025, 101891
- [32] R. Pitts et al., Nuclear Materials and Energy, Volume 42, March 2025, 101854
- [33] A. Gallo et al., Nuclear Materials and Energy, Volume 41, December 2024, 101741
- [34] J. Hobirk et al., this conference, EX-C 3489
- [35] K. Krieger et al., 9th Asia-Pacific Conference on Plasma Physics, September 21-26, 2025, Fukuoka International, Fukuoka, Japan
- [36] E. Geulin et al., this conference, EX-M 3072
- [37] R. Lunsford et al., Nuclear Materials and Energy, Volume 40, September 2024, 101726
- [38] E. Hodille et al, 20th International Conference on Plasma-Facing Materials and Components for Fusion Applications, Ljubljana, Slovenia, 19–23 May 2025D.
- [39] Matveev et a, Tritium removal from JET-ILW after T and D-T experimental campaigns, Nucl. Fusion 63 (2023) 112014
- [40] G Ghillardi et al 2025 Plasma Phys. Control. Fusion 67 055029
- [41]: C. Reux et al., Physica review letter 126, 175001 (2021) 10.1103/PhysRevLett.126.175001
- [42] S. Ratynskaya et al., Plasma Physics 2025, https://doi.org/10.48550/arXiv.2506.1041
- [43] N. Rivals et al 2025 Nucl. Fusion 65 026038
- [44] H. Bufferand, this conference, TH-P 2744
- [45] A. Mariani et al 2024 Nucl. Fusion 64 106024, DOI 10.1088/1741-4326/ad6ea0
- [46] X. Garbet et al., Nucl. Fusion 64 (2024) 106055, https://doi.org/10.1088/1741-4326/ad6e9f
- [47] L. Vermare et al. Nucl. Fusion, 62, 2021. doi:10.1088/1741-4326/ac3c85
- [48] R Varennes et al., Plasma Phys. Control. Fusion 66 (2024) 025003; https://doi.org/10.1088/1361-6587/ad1653
- [49] G. Dif Pradalier et al., Reviews of Modern Plasma Physics (2025) 9:23, https://doi.org/10.1007/s41614-025-00197-4
- [50] L. Delpech et al, FED 186 (2023) 113360
- [51] R. Ragona, et al., Fusion Engineering and Design, Volume 218, September 2025, 115168
- [52] X. Litaudon et al., this conference, EX-H 2770